Nuclear Tetrahedral Shapes from Multidimensionally-Constrained Covariant Density Functional Theories

Jie Zhao[a,b], Bing-Nan Lu[a,c], En-Guang Zhao[a,d] and Shan-Gui Zhou[a,d,e,f,*]

[a] *CAS Key Laboratory of Frontiers in Theoretical Physics, Institute of Theoretical Physics, Chinese Academy of Sciences, Beijing 100190, China*

[b] *Physics Department, Faculty of Science, University of Zagreb, Bijenicka 32, Zagreb 10000, Croatia*

[c] *Institut für Kernphysik (IKP-3) and Jülich Center for Hadron Physics, Forschungszentrum Jülich, D-52425 Jülich, Germany*

[d] *Center of Theoretical Nuclear Physics, National Laboratory of Heavy Ion Accelerator, Lanzhou 730000, China*

[e] *School of Physics, University of Chinese Academy of Sciences, Beijing 100049, China*

[f] *Synergetic Innovation Center for Quantum Effects and Application, Hunan Normal University, Changsha, 410081, China*

[*] *Email: sgzhou@itp.ac.cn*

Abstract

Many different shape degrees of freedom play crucial roles in determining the nuclear ground state and saddle point properties and the fission path. By breaking both the axial and the spatial reflection symmetries simultaneously, we have developed multidimensionally-constrained covariant density functional theories (MDC-CDFTs) in which all shape degrees of freedom $\beta_{\lambda\mu}$ with even μ, such as β_{20}, β_{22}, β_{30}, β_{32}, β_{40}, etc., are included self-consistently. The MDC-CDFT's have been applied to the study of fission barriers and potential energy surfaces of actinide nuclei, third minima in potential energy surfaces of light actinides, shapes and potential energy surfaces of superheavy nuclei, the Y_{32} correlations in $N = 150$ isotones and Zr isotopes, and shapes of hypernuclei. In this contribution we introduce MDC-CDFT's and focus on applications to tetrahedral nuclear shapes. With functionals DD-PC1 and PC-PK1, the ground state shape of ^{110}Zr is predicted to be tetrahedral so is that of ^{112}Zr with DD-PC1. The tetrahedral shape originates from large energy gaps around $Z = 40$ and $N = 70$ when the β_{32} distortion is allowed. With the functional DD-PC1, $\beta_{32} > 0.03$ and the energy gain due to the β_{32} distortion is larger than 300 keV for the ground states of ^{248}Cf and ^{250}Fm with $N = 150$.

Keywords: *Covariant density functional theory; tetrahedral shape; zirconium nuclei; transfermium nuclei*

Proceedings of the International Conference 'Nuclear Theory in the Supercomputing Era — 2016' (NTSE-2016), Khabarovsk, Russia, September 19–23, 2016. Eds. A. M. Shirokov and A. I. Mazur. Pacific National University, Khabarovsk, Russia, 2018, p. 159.

http://www.ntse-2016.khb.ru/Proc/Zhou.pdf.

1 Introduction

Most of known atomic nuclei have intrinsic shapes deviating from a sphere; in other words, they are deformed [1–3]. Nuclear deformations not only manifest themselves in collective states but also play important roles in determining nuclear potential energy surfaces (PES's) and fission barriers [4–6]. One way to describe nuclear deformations is by parameterizing the nuclear surface with a multipole expansion

$$R(\theta,\varphi) = R_0\left[1+\sum_{\lambda=1}^{\infty}\sum_{\mu=-\lambda}^{\lambda}\beta^*_{\lambda\mu}\,Y_{\lambda\mu}(\theta,\varphi)\right], \tag{1}$$

where $\beta_{\lambda\mu}$'s are deformation parameters. β_{20}, describing axial and quadrupole shapes, is the most important nuclear deformation. Beyond β_{20}, one can either go to higher order multipole with $\lambda > 2$, in particular $\beta_{\lambda 0}$ with odd λ corresponding to reflection-asymmetric nuclear shapes [7–9], or consider triaxial deformations $\beta_{\lambda\mu}$ with $\mu \neq 0$. Several interesting nuclear phenomena are related to triaxial or reflection asymmetric shapes such as the wobbling motion [2,10], chiral doublet bands [11–15], the termination of rotational bands [16], parity doublet bands [17–19], and the low-spin signature inversion [20–24]. Putting together β_{30} and β_{22}, it was revealed that the triaxial and octupole distortions both lower the second fission barrier of actinide nuclei considerably [25]. Furthermore, chirality-parity quartet bands are predicted in a nucleus with both a static triaxial deformation (β_{22}) and an octupole deformation (β_{30}) [26]. The triaxiality and reflection asymmetry are combined in deformations characterized by $\beta_{\lambda\mu}$ with odd λ and nonzero μ. Among such deformations, the β_{32} deformation is of particular interest and has been investigated extensively [27–36]. A nucleus with a pure β_{32} deformation, i. e., $\beta_{\lambda\mu} = 0$ if $\lambda \neq 3$ and $\mu \neq 2$, has a tetrahedral shape with the symmetry group T_d^D. The study of single-particle structure of nuclei with tetrahedral symmetry predicted large energy gaps at $Z(N) = 16$, 20, 32, 40, 56–58, 70, and 90–94 and $N = 112$ and 136/142 [29, 32, 37–46]. These shell gaps may be comparable to or even stronger than those at spherical shapes. Thus, a nucleus with proton and/or neutron numbers equal to these numbers may have a static tetrahedral shape or strong tetrahedral correlations.

For the study of nuclear ground states, shape isomers and PES's, it is desirable to have microscopic and self-consistent models which incorporate all known important shape degrees of freedom. We have developed such a model, the so-called multidimensionally-constrained covariant density functional theories (MDC-CDFT's), by breaking the reflection and axial symmetries simultaneously. Within the MDC-CDFT's, the nuclear shape is assumed to be invariant under the reversion of x and y axes, i. e., the intrinsic symmetry group is V_4 and all shape degrees of freedom $\beta_{\lambda\mu}$ with even μ (β_{20}, β_{22}, β_{30}, β_{32}, β_{40}, ...) are included self-consistently. The MDC-CDFT's consist of two types of models: the multidimensionally-constrained relativistic mean field (MDC-RMF) model and the multidimensionally-constrained relativistic Hartree–Bogoliubov (MDC-RHB) model. In the MDC-RMF model, the BCS approach has been implemented for the particle-particle (pp) channel. This model has been used to study potential energy surfaces and fission barriers of actinides [25, 47–51], the spontaneous fission of several fermium isotopes [52], the Y_{32} correlations in $N = 150$ isotones [53], and shapes of hypernuclei [54,55], see Refs. [6,56,57] for recent reviews. The Bogoliubov transformation generalizes the BCS quasi-particle concept and provides a unified description of particle-hole (ph) and pp correlations on the mean-field

level. In the MDC-RHB model, pairing correlations are treated by making the Bogoliubov transformation and a separable pairing force of a finite range [58–62] is adopted. The MDC-RHB model has been used to study the spontaneous fission of fermium isotopes [63] and neutron-rich Zr nuclei [64].

In this contribution, we present briefly the formalism of the MDC-RHB model and some results of neutron-rich Zr nuclei and $N = 150$ isotones. The formulae of the MDC-RHB model are given in Section 2. The results and discussions are presented in Section 3. A summary is given in Section 4.

2 Formalism

In the CDFT [65–74], there are four types of covariant density functionals: the meson exchange or point-coupling nucleon interactions combined with nonlinear or density dependent couplings [75–81] (see Ref. [82] for recent reviews). All these four types of functionals have been implemented in the MDC-RHB model. In this Section, we mainly present the formalism of the RHB model with density dependent point-couplings. The starting point of the RHB model with the density dependent point-couplings is the following Lagrangian,

$$\begin{aligned}\mathcal{L} = \bar{\psi}(i\gamma_\mu\partial^\mu - M)\psi - \frac{1}{2}\alpha_S(\hat{\rho})\,\rho_S^2 - \frac{1}{2}\alpha_V(\hat{\rho})\,j_V^2 - \frac{1}{2}\alpha_{TV}(\hat{\rho})\,\vec{j}_{TV}^{\,2} \\ - \frac{1}{2}\delta_S(\partial_\nu\rho_S)(\partial^\nu\rho_S) - e\frac{1-\tau_3}{2}A_\mu\,j_V^\mu - \frac{1}{4}F^{\mu\nu}F_{\mu\nu},\end{aligned} \quad (2)$$

where M is the nucleon mass, $\alpha_S(\hat{\rho})$, $\alpha_V(\hat{\rho})$, and $\alpha_{TV}(\hat{\rho})$ are density-dependent couplings for different channels, δ_S is the coupling constant of the derivative term, and e is the electric charge. ρ_S, j_V, and $\vec{j}_{TV}$ are the iso-scalar density, the iso-scalar current, and the iso-vector current, respectively.

With the Green's function technique, one can derive the Dirac–Hartree–Bogoliubov equation [67, 83],

$$\int d^3\boldsymbol{r}' \begin{pmatrix} h-\lambda & \Delta \\ -\Delta^* & -h+\lambda \end{pmatrix} \begin{pmatrix} U_k \\ V_k \end{pmatrix} = E_k \begin{pmatrix} U_k \\ V_k \end{pmatrix}, \quad (3)$$

where E_k is the quasiparticle energy, λ is the chemical potential, and $\hat{h}$ is the single-particle Hamiltonian,

$$\hat{h} = \boldsymbol{\alpha}\cdot[\boldsymbol{p} - \boldsymbol{V}(\boldsymbol{r})] + \beta[M + S(\boldsymbol{r})] + V_0(\boldsymbol{r}) + \Sigma_R(\boldsymbol{r}), \quad (4)$$

S, V^μ, and Σ_R are the scalar potential, the vector potential, and the rearrangement terms. The pairing potential reads

$$\Delta_{ff}(\boldsymbol{r}_1\sigma_1, \boldsymbol{r}_2\sigma_2) = \int d^3\boldsymbol{r}_1' d^3\boldsymbol{r}_2' \sum_{\sigma_1'\sigma_2'} V^{\rm pp}_{ff,ff}(\boldsymbol{r}_1\sigma_1, \boldsymbol{r}_2\sigma_2, \boldsymbol{r}_1'\sigma_1', \boldsymbol{r}_2'\sigma_2')\,\kappa_{ff}(\boldsymbol{r}_1'\sigma_1', \boldsymbol{r}_2'\sigma_2'), \quad (5)$$

where f and g are used to represent the large and small components of the Dirac spinor, $V^{\rm pp}$ is the effective pairing interaction and $\kappa(\boldsymbol{r}_1\sigma_1, \boldsymbol{r}_2\sigma_2)$ is the pairing tensor.

The RHB equation (3) is solved by expanding the large and small components of the spinors $U_k(\boldsymbol{r}\sigma)$ and $V_k(\boldsymbol{r}\sigma)$ in an axially-deformed harmonic oscillator (ADHO)

basis [84],

$$U_k(\boldsymbol{r}\sigma) = \begin{pmatrix} \sum_\alpha f_U^{k\alpha}\,\Phi_\alpha(\boldsymbol{r}\sigma) \\ \sum_\alpha g_U^{k\alpha}\,\Phi_\alpha(\boldsymbol{r}\sigma) \end{pmatrix}, \quad V_k(\boldsymbol{r}\sigma) = \begin{pmatrix} \sum_\alpha f_V^{k\alpha}\,\Phi_\alpha(\boldsymbol{r}\sigma) \\ \sum_\alpha g_V^{k\alpha}\,\Phi_\alpha(\boldsymbol{r}\sigma) \end{pmatrix}, \tag{6}$$

where $\Phi_\alpha(\boldsymbol{r}\sigma)$ are eigensolutions of the Schrödinger equation with the ADHO potential,

$$\left[-\frac{\hbar^2}{2M}\nabla^2 + V_B(\rho,z)\right]\Phi_\alpha(\boldsymbol{r}\sigma) = E_\alpha\Phi_\alpha(\boldsymbol{r}\sigma), \tag{7}$$

and

$$V_B(\rho,z) = \frac{1}{2}M(\omega_\rho^2\rho^2 + \omega_z^2 z^2). \tag{8}$$

In Eq. (6), $\alpha = \{n_z, n_r, m_l, m_s\}$ is the collection of quantum numbers, and ω_z and ω_ρ are the oscillator frequencies along and perpendicular to the symmetry (z) axis, respectively. The V_4 symmetry is imposed in the MDC-CDFT [6]. Thus we expand the potentials and the densities in terms of the Fourier series,

$$f(\rho,\varphi,z) = f_0(\rho,z)\frac{1}{\sqrt{2\pi}} + \sum_{n=1}^{\infty} f_n(\rho,z)\frac{1}{\sqrt{\pi}}\cos(2n\varphi), \tag{9}$$

In the *pp* channel, we use a separable pairing force of a finite range [58–62]. The matrix element $\bar{V}^{\rm pp}_{12,1'2'} = V^{\rm pp}_{12,1'2'} - V^{\rm pp}_{12,2'1'}$ in the center of mass frame reads

$$V_{12,1'2'} = -2\sqrt{2}G\sum_{N_zN_pM_p}\left(W_{12}^{N_zN_pM_p}\right)^* W_{1'2'}^{N_zN_pM_p}, \tag{10}$$

where

$$\begin{aligned} W_{12}^{N_zN_pM_p} = {} & \delta_{K_1+K_2,M_p}\,\delta_{\pi_1\pi_2,(-1)^{N_z+|M_p|}}\,\tau_1\frac{1}{\sqrt{2}}C_1C_2 \\ & \times\left(\sum_{n_z} M^{n_{z_1}n_{z_2}}_{N_zn_z}V_{n_z}\right)\left(\sum_{n_p} M^{n_{r_1}m_1n_{r_2}m_2}_{N_pM_pn_p0}U_{n_p}\right), \end{aligned} \tag{11}$$

and

$$\begin{aligned} V_{n_z} &= \frac{1}{(4\pi a^2)^{1/2}}\int_{-\infty}^{\infty} dz\, e^{-\frac{z^2}{2a^2}}\phi_{n_z}(z), \\ U_{n_p} &= \frac{\sqrt{2\pi}}{4\pi a^2}\int_0^{\infty} d\rho\rho\, e^{-\frac{\rho^2}{2a^2}}R^0_{n_p}(\rho). \end{aligned} \tag{12}$$

$M^{n_{z_1}n_{z_2}}_{N_zn_z}$ and $M^{n_{r_1}m_1n_{r_2}m_2}_{N_pM_pn_pm_p}$ are the Talmi–Moshinski brackets. The pairing field and pairing energy can be also written in a separable form as

$$\Delta_{12} = \sum_{1'2'} V_{12,1'2'}\,\kappa_{1'2'} = -2\sqrt{2}G\sum_{N_z}\sum_{N_pM_p}\left(W_{12}^{N_zN_pM_p}\right)^* P^{N_zN_pM_p}, \tag{13}$$

$$E_{\rm pair} = \frac{1}{2}\sum_{12,1'2'} V_{12,1'2'}\,\kappa^*_{12}\kappa_{1'2'} = -\sqrt{2}G\sum_{N_z}\sum_{N_pM_p}|P^{N_zN_pM_p}|^2, \tag{14}$$

where

$$P^{N_z N_p M_p} = \sum_{12} W_{12}^{N_z N_p M_p} \kappa_{12}. \tag{15}$$

The details of the derivation are given in Appendices of Refs. [48, 64].

The total energy of the nucleus reads

$$\begin{aligned} E_{\rm total} = \int d^3\boldsymbol{r} \Bigg\{ & \sum_k v_k^2 \, \psi_k^\dagger \left(\boldsymbol{\alpha}\cdot\boldsymbol{p} + \beta M_{\rm B}\right) \psi_k \\ & + \frac{1}{2}\alpha_S \rho_S^2 + \frac{1}{2}\alpha_V \rho_V^2 + \frac{1}{2}\alpha_{TS} \rho_{TS}^2 + \frac{1}{2}\alpha_{TV} \rho_{TV}^2 \\ & + \frac{1}{3}\beta_S \rho_S^3 + \frac{1}{4}\gamma_S \rho_S^4 + \frac{1}{4}\gamma_V \rho_V^4 \\ & + \frac{1}{2}\delta_S \rho_S \Delta\rho_S + \frac{1}{2}\delta_V \rho_V \Delta\rho_V \\ & + \frac{1}{2}\delta_{TS} \rho_{TS} \Delta\rho_{TS} + \frac{1}{2}\delta_{TV} \rho_{TV} \Delta\rho_{TV} + \frac{1}{2} e \rho_C A \Bigg\} \\ & + E_{\rm pair} + E_{\rm c.m.}, \end{aligned} \tag{16}$$

where the center of mass correction $E_{\rm c.m.}$ can be calculated either phenomenologically or microscopically. The intrinsic multipole moments are calculated as

$$Q_{\lambda\mu}^\tau = \int d^3\boldsymbol{r} \, \rho_V^\tau(\boldsymbol{r}) \, r^\lambda \, Y_{\lambda\mu}(\Omega), \tag{17}$$

where $Y_{\lambda\mu}(\Omega)$ are the spherical harmonics and τ refers to the proton, neutron, or the whole nucleus. The deformation parameter $\beta_{\lambda\mu}$ is obtained from the corresponding multipole moment by

$$\beta_{\lambda\mu}^\tau = \frac{4\pi}{3 N_\tau R^\lambda} Q_{\lambda\mu}, \tag{18}$$

where $R = 1.2 \times A^{1/3}$ fm and N_τ is the number of proton, neutron, or nucleons.

3 Results and discussions

3.1 Tetrahedral shapes of neutron-rich Zr isotopes

In Ref. [64], one-dimensional potential energy curves ($E \sim \beta_{20}$) for even-even Zr nuclei with $100 \leq A \leq 114$ were calculated with functionals DD-PC1 [61] and PC-PK1 [85]. To investigate different roles played by the nonaxiality and reflection asymmetry, calculations are preformed with different symmetries imposed: i) axial and reflection symmetry, ii) axial symmetry and reflection asymmetry, and iii) nonaxial and reflection asymmetry; the results are shown in Figs. 1 and 2 by dotted, dash-dotted, and solid lines respectively.

In Fig. 1, we present the results obtained with the functional DD-PC1. We can see that if nuclei are allowed to be reflection asymmetric but axial symmetric, the energy of the minimum with $\beta_{20} \approx 0$ for $^{106-114}$Zr is lowered substantially by the β_{30} distortion. Due to this lowering effect, the energy of the minimum with the pear-like shape ($\beta_{20} \approx 0$, $\beta_{30} \neq 0$) is lower than the minimum with oblate or prolate shape for ^{110}Zr, ^{112}Zr, and ^{114}Zr. When the β_{32} deformation is allowed in the calculations,

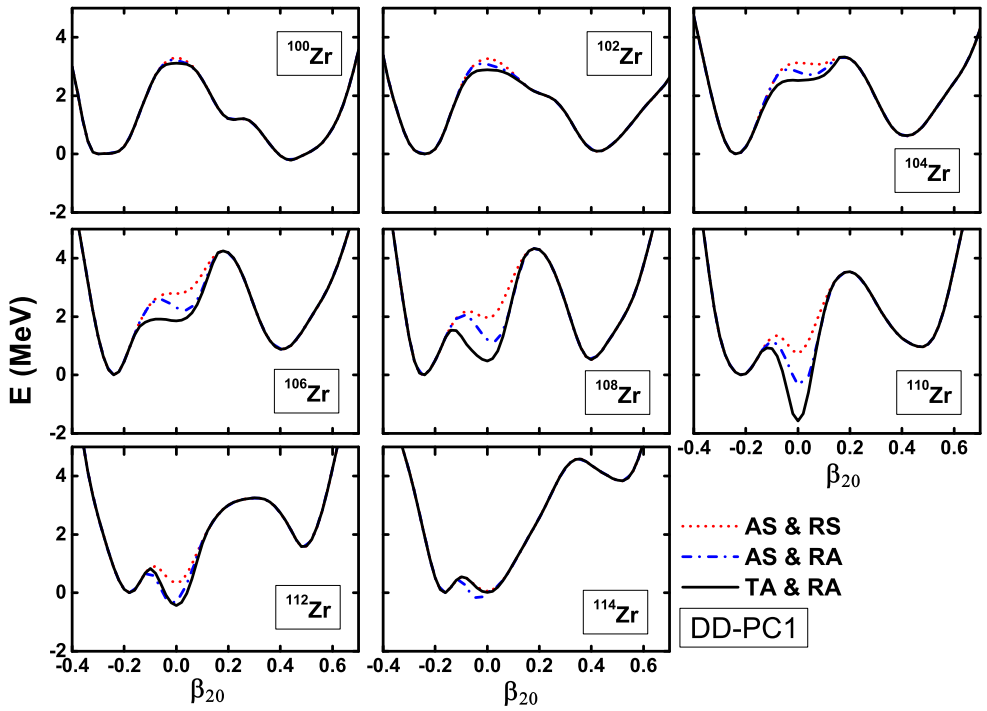

Figure 1: Potential energy curves for Zr isotopes with the functional DD-PC1. The energy is normalized with respect to the oblate minimum for each nucleus. Various symmetries are imposed in the calculations: axial symmetry (AS), triaxial (TA), reflection symmetry (RS) and reflection asymmetry (RA). Taken from Ref. [64].

both axial and reflection symmetries are broken. The β_{32} distortion effect is more pronounced than that of the β_{30} deformation for most of these nuclei. The energy of the minimum with $\beta_{20} \approx 0$ for $^{106-112}$Zr is lowered much. A tetrahedral ground state is predicted for ^{110,112}Zr. For ^{114}Zr, the predicted pear-like shape is lower in energy than the tetrahedral shape. From Fig. 1, we conclude that the β_{32} distortion effect is the most pronounced for ^{110}Zr where the inclusion of the β_{32} deformation lowers the energy of the minimum around $\beta_{20} = 0$ by about 2 MeV.

In Fig. 2, the results obtained with the functional PC-PK1 are presented. The β_{30} and β_{32} distortion effects are observed around $\beta_{20} = 0$ for ^{108,110}Zr. The most pronounced distortion effects are predicted for ^{110}Zr which is consistent with the results obtained from DD-PC1. As a result, the ground states of ^{108,110}Zr are predicted to have tetrahedral shapes and there also exist pear-like isomeric states. Neither β_{30} nor β_{32} distortions have influences on the PEC's of ^{112,114}Zr.

In Ref. [64], we also examined the origin of the strong β_{32} effect around ^{110}Zr. We found that the formation of the tetrahedral ground state around ^{110}Zr can be traced back to the large energy gaps at $Z = 40$ and $N = 70$ in the single-particle levels when the β_{32} deformation is included. In Fig. 3, we show the single-particle levels of ^{110}Zr near the Fermi surface as functions of β_{32} with β_{20} fixed at zero. Due to the tetrahedral symmetry, the single-particle levels are split into multiplets with

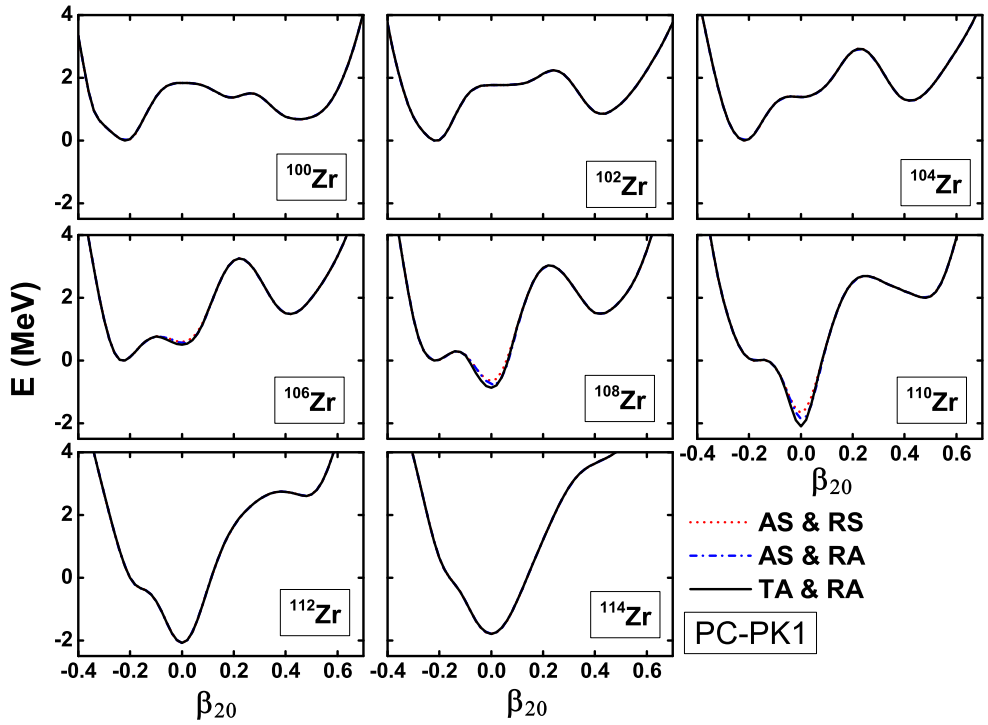

Figure 2: Potential energy curves for Zr isotopes with the functional PC-PK1. The energy is normalized with respect to the oblate minimum for each nucleus. Various symmetries are imposed in the calculations: axial symmetry (AS), triaxial (TA), reflection symmetry (RS) and reflection asymmetry (RA).

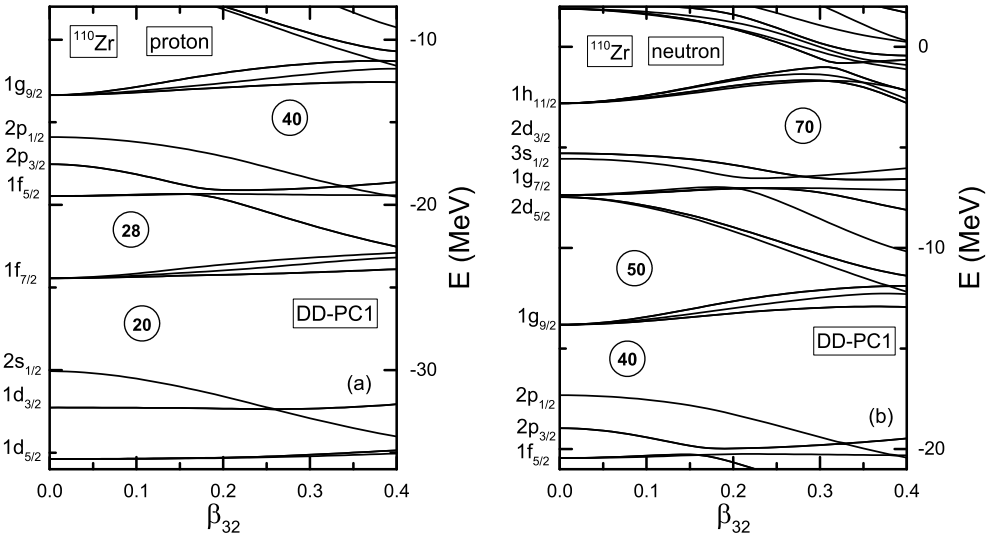

Figure 3: Single-particle levels near the Fermi surface for protons (a) and neutrons (b) of ^{110}Zr as functions of β_{32} with β_{20} fixed at zero. Taken from Ref. [64].

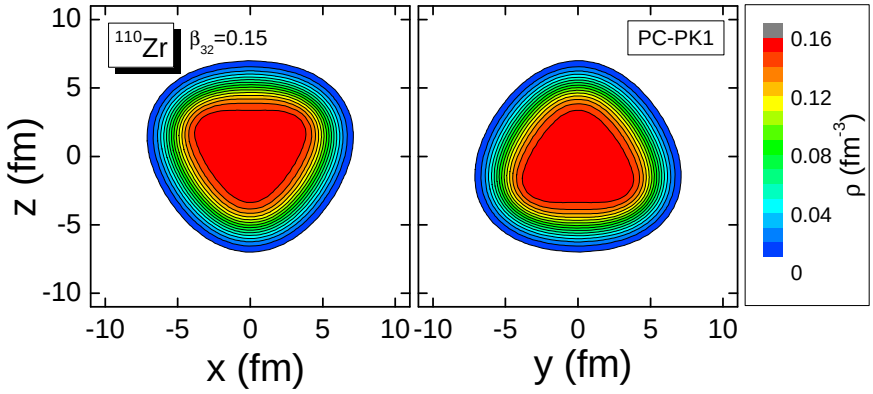

Figure 4: Ground state density profile of ^{110}Zr in the (x, z) and (y, z) planes obtained for the functional PC-PK1.

degeneracies equal to the irreducible representations of the T_d^D group. For protons, as shown in Fig. 3(a), the magic gap $Z = 20$ is enhanced while the gap at $Z = 28$ is suppressed as β_{32} increases. At $Z = 40$ a large energy gap shows up as β_{32} increases. From Fig. 3(b) we can see that large energy gaps appear at $N = 40$ and 70 while a spherical magic gap at $N = 50$ is suppressed as β_{32} increases. Due to the large energy gaps at $Z = 40$ and $N = 70$, a strong β_{32} effect is expected for ^{110}Zr and nearby nuclei. The ground state density profile of ^{110}Zr obtained from PC-PK1 is shown in Fig. 4.

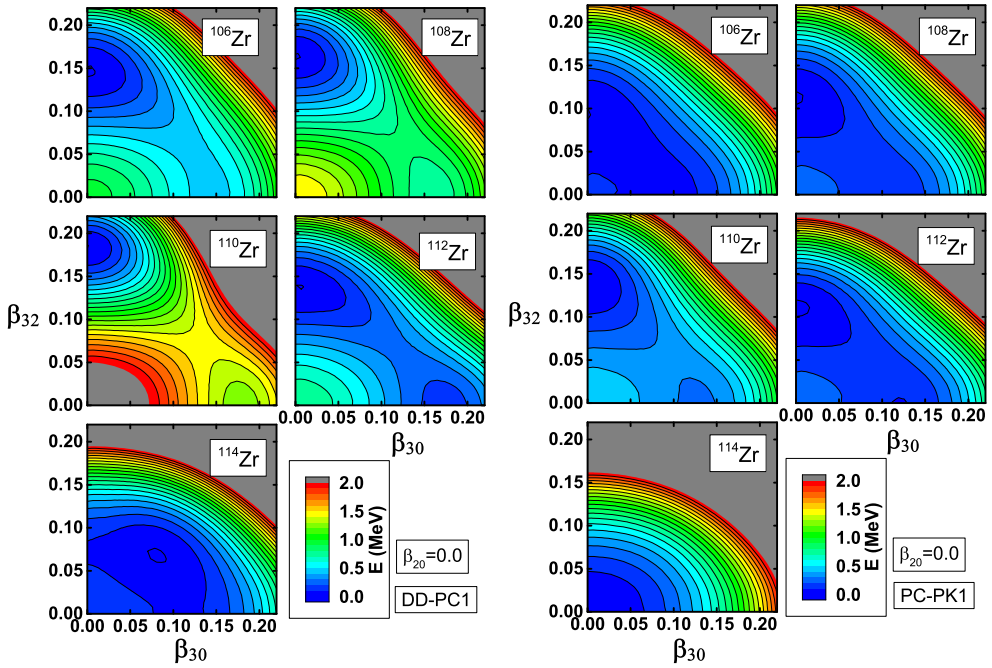

Figure 5: Potential energy surfaces of $^{106-114}$Zr in the (β_{30}, β_{32}) plane with β_{20} fixed at zero. The contour interval is 0.1 MeV. Taken from Ref. [64].

The potential energy surfaces (PES) of $^{106-114}$Zr in the (β_{30}, β_{32}) plane with β_{20} fixed at zero are shown in Fig. 5. It is clearly seen that the minima with tetrahedral shapes are deeper than that of pear-like shapes for $^{106-112}$Zr with both functionals. The barriers separating the pear-like and tetrahedral minima are very low. For ^{106}Zr, the barrier is almost invisible with both functionals. For ^{108}Zr and ^{112}Zr, the barriers predicted by DD-PC1 are less than 0.2 MeV while the barriers predicted by PC-PK1 are around 0.1 MeV. For ^{110}Zr, the barrier predicted by DD-PC1 is higher but still less than 0.3 MeV, while the barrier height from the calculations with PC-PK1 is less than 0.2 MeV. In this sense, the pear-like isomeric states are rather unstable.

3.2 Non-axial octupole shapes in $N = 150$ isotones

In Ref. [53], the non-axial reflection-asymmetric β_{32} shape in some transfermium nuclei with $N = 150$, namely, in ^{246}Cm, ^{248}Cf, ^{250}Fm and ^{252}No, were investigated within the MDC-RMF model. The parameter set DD-PC1 was used [61]. One-dimensional potential energy curves (E vs β_{32}) are shown in Fig. 6. For the ground states of ^{248}Cf and ^{250}Fm, the non-axial octupole deformation parameter $\beta_{32} > 0.03$ and the energy gain due to the β_{32} distortion is larger than 300 keV. In ^{246}Cm and ^{252}No, shallow β_{32} minima are found.

The triaxial octupole Y_{32} effects stem from the coupling between pairs of single-particle orbits with $\Delta j = \Delta l = 3$ and $\Delta K = 2$ where j and l are respectively the single-particle total and orbital angular momenta and K is the projection of j on the symmetry axis. In Fig. 7, we show the proton and neutron single-particle levels near the Fermi surface for ^{248}Cf as a function of β_{32} with β_{20} fixed at 0.3. It has been shown that the spherical proton orbitals $\pi 2f_{7/2}$ and $\pi 1i_{13/2}$ are very close to each other. This near degeneracy results in octupole correlations. As seen in the left panel of Fig. 7, two proton levels, [521]3/2 originating from $2f_{7/2}$ and [633]7/2 originating from $1i_{13/2}$, satisfying the $\Delta j = \Delta l = 3$ and $\Delta K = 2$ condition, are very close to each other at $\beta_{20} = 0.3$. Therefore the non-axial octupole Y_{32} develops, and an energy gap appears at $Z = 98$ as β_{32} increases from zero. Similarly, the spherical neutron orbitals $\nu 2g_{9/2}$ and $\nu 1j_{15/2}$ are very close to each other. The neutron levels [734]9/2 originating from $1j_{15/2}$ and [622]5/2 originating from $2g_{9/2}$ are also close lying just above and below the Fermi surface. This leads to the development of a gap

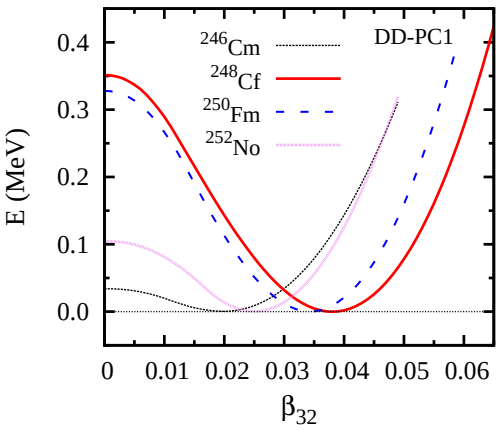

Figure 6: Binding energy E (relative to the ground state) for $N = 150$ isotones ^{246}Cm, ^{248}Cf, ^{250}Fm, and ^{252}No as functions of the non-axial octupole deformation parameter β_{32}. Taken form Ref. [53].

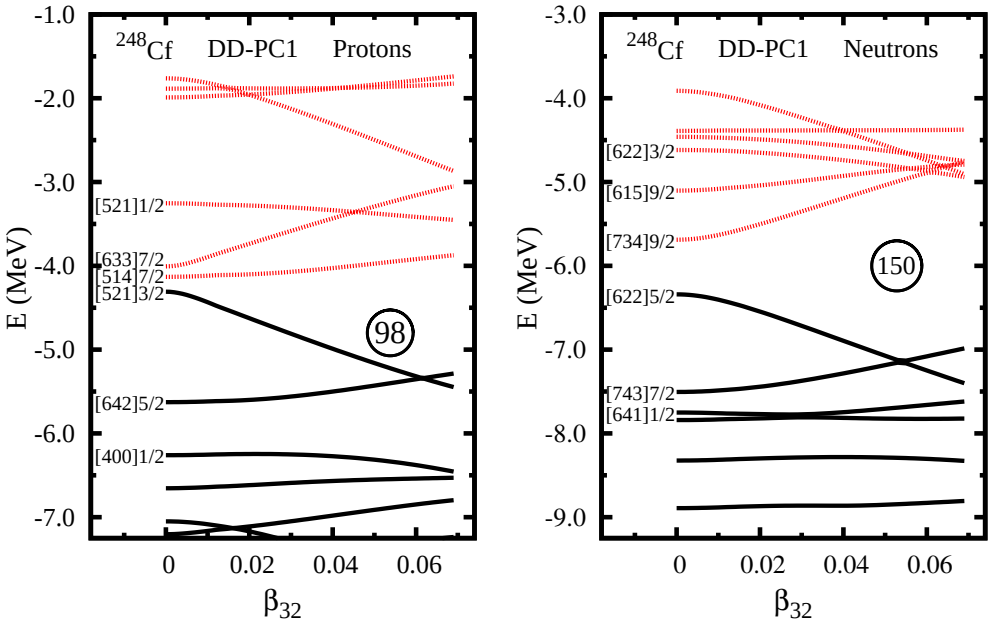

Figure 7: Single-particle levels near the Fermi surface for protons and neutrons of ^{248}Cf as functions of β_{32} with β_{20} fixed at 0.3.

at $N = 150$ with β_{32} increasing. The Y_{32} correlation in $N = 150$ isotones is caused by both protons and neutrons, and the correlation in ^{248}Cf is the most pronounced.

4 Summary

In this contribution we present briefly the formalism and some applications of the multidimensionally-constrained covariant density functional theories (MDC-CDFT) in which all shape degrees of freedom like $\beta_{\lambda\mu}$ deformations with even μ are allowed. We have calculated the potential energy curves (E vs β_{32}) of neutron-rich even-even Zr isotopes within the MDC-RHB model. It is found that the β_{32} deformation plays a very important role in the isomeric or ground states of these nuclei, especially for nuclei around $N = 70$. The ground state shape of ^{110}Zr is predicted to be tetrahedral with both functionals, DD-PC1 and PC-PK1. ^{108}Zr is also predicted to have the tetrahedral ground state with the functional PC-PK1 and ^{112}Zr is predicted to have the tetrahedral ground state with the functional DD-PC1. The strong β_{32} distortion effect is caused by the large energy gaps at $Z = 40$ and $N = 70$. The non-axial reflection-asymmetric β_{32} shape in some transfermium nuclei with $N = 150$, namely, in ^{246}Cm, ^{248}Cf, ^{250}Fm and ^{252}No, are studied. Due to the interaction between a pair of neutron orbitals, [734]9/2 originating from $\nu j_{15/2}$ and [622]5/2 originating from $\nu g_{9/2}$, and that of a pair of proton orbitals, [521]3/2 originating from $\pi f_{7/2}$ and [633]7/2 originating from $\pi i_{13/2}$, rather strong non-axial octupole Y_{32} effects have been found in ^{248}Cf and ^{250}Fm which are both well-deformed with large axial-quadrupole deformations, $\beta_{20} \approx 0.3$.

Acknowledgments

This work has been supported by the National Key Basic Research Program of China (Grant No. 2013CB834400), the National Natural Science Foundation of China (Grant Nos. 11120101005, 11275248, 11475115, 11525524 and 11621131001), and the Knowledge Innovation Project of the Chinese Academy of Sciences (Grant No. KJCX2-EW-N01). The computational results presented in this work have been obtained using the High-performance Computing Cluster of KLTP/ITP-CAS and the ScGrid of the Supercomputing Center, Computer Network Information Center of the Chinese Academy of Sciences.

References

[1] A. Bohr and B. Mottelson, *Nuclear structure. Vol I.* World Scientific, Singapore, 1998.

[2] A. Bohr and B. Mottelson, *Nuclear structure. Vol II.* World Scientific, Singapore, 1998.

[3] P. Ring and P. Schuck, *The nuclear many-body problem.* Springer-Verlag, Berlin, Heidelberg, 1980.

[4] S. Frauendorf, Rev. Mod. Phys. **73**, 463 (2001).

[5] W. Nazarewicz, in *An advanced course in modern nuclear physics*, eds. J. Arias and M. Lozano, Lecture Notes Phys. **581**, 102. Springer, Berlin, Heidelberg, 2001.

[6] S.-G. Zhou, Phys. Scripta **91**, 063008 (2016).

[7] P. A. Butler and W. Nazarewicz, Rev. Mod. Phys. **68**, 349 (1996).

[8] P. Möller, R. Bengtsson, B. G. Carlsson, P. Olivius, T. Ichikawa, H. Sagawa and A. Iwamoto, At. Data Nucl. Data Tables **94**, 758 (2008).

[9] S. E. Agbemava, A. V. Afanasjev and P. Ring, Phys. Rev. C **93**, 044304 (2016).

[10] S. W. Odegard, G. B. Hagemann, D. R. Jensen, M. Bergstroem, B. Herskind, G. Sletten, S. Toermaenen, J. N. Wilson, P. O. Tjom, I. Hamamoto, K. Spohr, H. Huebel, A. Goergen, G. Schoenwasser, A. Bracco, S. Leoni, A. Maj, C. M. Petrache, P. Bednarczyk and D. Curien, Phys. Rev. Lett. **86**, 5866 (2001).

[11] S. Frauendorf and J. Meng, Nucl. Phys. A **617**, 131 (1997).

[12] K. Starosta, T. Koike, C. J. Chiara, D. B. Fossan, D. R. LaFosse, A. A. Hecht, C. W. Beausang, M. A. Caprio, J. R. Cooper, R. Krucken, J. R. Novak, N. V. Zamfir, K. E. Zyromski, D. J. Hartley, D. L. Balabanski, Jing-ye Zhang, S. Frauendorf and V. I. Dimitrov, Phys. Rev. Lett. **86**, 971 (2001).

[13] J. Meng, J. Peng, S. Q. Zhang and S.-G. Zhou, Phys. Rev. C **73**, 037303 (2006).

[14] J. Meng and S. Q. Zhang, J. Phys. G **37**, 064025 (2010).

[15] J. Meng, S.-Q. Zhang and P. Zhao, *Novel rotational excitations*, in *Relativistic mean field description of exotic nuclei, chap. 9*, Int. Rev. Nucl. Phys. **10**, 355. World Scientific, 2016.

[16] A. V. Afanasjev, D. B. Fossan, G. J. Lane and I. Ragnarsson, Phys. Rep. **322**, 1 (1999).

[17] L. P. Gaffney, P. A. Butler, M. Scheck, A. B. Hayes, F. Wenander, M. Albers, B. Bastin, C. Bauer, A. Blazhev, S. Bonig, N. Bree, J. Cederkall, T. Chupp, D. Cline, T. E. Cocolios, T. Davinson, H. De Witte, J. Diriken, T. Grahn, A. Herzan, M. Huyse, D. G. Jenkins, D. T. Joss, N. Kesteloot, J. Konki, M. Kowalczyk, T. Kroll, E. Kwan, R. Lutter, K. Moschner, P. Napiorkowski, J. Pakarinen, M. Pfeiffer, D. Radeck, P. Reiter, K. Reynders, S. V. Rigby, L. M. Robledo, M. Rudigier, S. Sambi, M. Seidlitz, B. Siebeck, T. Stora, P. Thoele, P. Van Duppen, M. J. Vermeulen, M. von Schmid, D. Voulot, N. Warr, K. Wimmer, K. Wrzosek-Lipska, C. Y. Wu and M. Zielinska, Nature **497**, 199 (2013).

[18] B. Bucher, S. Zhu, C. Y. Wu, R. V. F. Janssens, D. Cline, A. B. Hayes, M. Albers, A. D. Ayangeakaa, P. A. Butler, C. M. Campbell, M. P. Carpenter, C. J. Chiara, J. A. Clark, H. L. Crawford, M. Cromaz, H. M. David, C. Dickerson, E. T. Gregor, J. Harker, C. R. Hoffman, B. P. Kay, F. G. Kondev, A. Korichi, T. Lauritsen, A. O. Macchiavelli, R. C. Pardo, A. Richard, M. A. Riley, G. Savard, M. Scheck, D. Seweryniak, M. K. Smith, R. Vondrasek and A. Wiens, Phys. Rev. Lett. **116**, 112503 (2016).

[19] X. C. Chen, J. Zhao, C. Xu, H. Hua, T. M. Shneidman, S. G. Zhou, X. G. Wu, X. Q. Li, S. Q. Zhang, Z. H. Li, W. Y. Liang, J. Meng, F. R. Xu, B. Qi, Y. L. Ye, D. X. Jiang, Y. Y. Cheng, C. He, J. J. Sun, R. Han, C. Y. Niu, C. G. Li, P. J. Li, C. G. Wang, H. Y. Wu, Z. H. Li, H. Zhou, S. P. Hu, H. Q. Zhang, G. S. Li, C. Y. He, Y. Zheng, C. B. Li, H. W. Li, Y. H. Wu, P. W. Luo and J. Zhong, Phys. Rev. C **94**, 021301(R) (2016).

[20] Y. Liu, Y. Ma, H. Yang, and S. Zhou, Phys. Rev. C **52**, 2514 (1995).

[21] Y. Liu, J. Lu, Y. Ma, S. Zhou and H. Zheng, Phys. Rev. C **54**, 719 (1996).

[22] S. G. Zhou, Y. Z. Liu, Y. J. Ma and C. X. Yang, J. Phys. G **22**, 415 (1996).

[23] L. L. Riedinger, H. Q. Jin, W. Reviol, J.-Y. Zhang, R. A. Bark, G. B. Hagemann and P. B. Semmes, Prog. Part. Nucl. Phys. **38**, 251 (1997).

[24] Y. Liu, J. Lu, Y. Ma, G. Zhao, H. Zheng and S. Zhou, Phys. Rev. C **58**, 1849 (1998).

[25] B.-N. Lu, E.-G. Zhao and S.-G. Zhou, Phys. Rev. C **85**, 011301(R) (2012).

[26] C. Liu, S. Y. Wang, R. A. Bark, S. Q. Zhang, J. Meng, B. Qi, P. Jones, S. M. Wyngaardt, J. Zhao, C. Xu, S.-G. Zhou, S. Wang, D. P. Sun, L. Liu, Z. Q. Li, N. B. Zhang, H. Jia, X. Q. Li, H. Hua, Q. B. Chen, Z. G. Xiao, H. J. Li, L. H. Zhu, T. D. Bucher, T. Dinoko, J. Easton, K. Juhász, A. Kamblawe, E. Khaleel, N. Khumalo, E. A. Lawrie, J. J. Lawrie, S. N. T. Majola, S. M. Mullins, S. Murray, J. Ndayishimye, D. Negi, S. P. Noncolela,

S. S. Ntshangase, B. M. Nyakó, J. N. Orce, P. Papka, J. F. Sharpey-Schafer, O. Shirinda, P. Sithole, M. A. Stankiewicz and M. Wiedeking, Phys. Rev. Lett. **116**, 112501 (2016).

[27] I. Hamamoto, B. Mottelson, H. Xie and X. Z. Zhang, Z. Phys. D **21**, 163 (1991).

[28] J. Skalski, Phys. Rev. C **43**, 140 (1991).

[29] X. Li and J. Dudek, Phys. Rev. C **49**, R1250 (1994).

[30] S. Takami, K. Yabana and M. Matsuo, Phys. Lett. B **431**, 242 (1998).

[31] M. Yamagami, K. Matsuyanagi and M. Matsuo, Nucl. Phys. A **693**, 579 (2001).

[32] J. Dudek, A. Gozdz, N. Schunck and M. Miskiewicz, Phys. Rev. Lett. **88**, 252502 (2002).

[33] J. Dudek, D. Curien, N. Dubray, J. Dobaczewski, V. Pangon, P. Olbratowski and N. Schunck, Phys. Rev. Lett. **97**, 072501 (2006).

[34] P. Olbratowski, J. Dobaczewski, P. Powalowski, M. Sadziak and K. Zberecki, Int. J. Mod. Phys. E **15**, 333 (2006).

[35] K. Zberecki, P. Magierski, P.-H. Heenen and N. Schunck, Phys. Rev. C **74**, 051302(R) (2006).

[36] J. Dudek, A. Gozdz, K. Mazurek and H. Molique, J. Phys. G **37**, 064032 (2010).

[37] J. Dudek, J. Dobaczewski, N. Dubray, A. Gozdz, V. Pangon and N. Schunck, Int. J. Mod. Phys. E **16**, 516 (2007).

[38] J. Dudek, A. Gozdz and N. Schunck, Acta Phys. Pol. B **34**, 2491 (2003).

[39] W. D. Heiss, R. A. Lynch and R. G. Nazmitdinov, Phys. Rev. C **60**, 034303 (1999).

[40] K. Arita and Y. Mukumoto, Phys. Rev. C **89**, 054308 (2014).

[41] N. Schunck, J. Dudek, A. Gozdz and P. H. Regan, Phys. Rev. C **69**, 061305(R) (2004).

[42] J. Dudek, D. Curien, D. Rouvel, K. Mazurek, Y. R. Shimizu and S. Tagami, Phys. Scripta **89**, 054007 (2014).

[43] K. Zberecki, P.-H. Heenen and P. Magierski, Phys. Rev. C **79**, 014319 (2009).

[44] R. Bijker and F. Iachello, Phys. Rev. Lett. **112**, 152501 (2014).

[45] Y. Chen and Z. Gao, Nucl. Phys. Rev. **30**, 278 (2013).

[46] Y. S. Chen and Z.-C. Gao, Nucl. Phys. A **834**, 378c (2010).

[47] B.-N. Lu, J. Zhao, E.-G. Zhao and S.-G. Zhou, J. Phys. Conf. Ser. **492**, 012014 (2014).

[48] B.-N. Lu, J. Zhao, E.-G. Zhao and S.-G. Zhou, Phys. Rev. C **89**, 014323 (2014).

[49] B.-N. Lu, J. Zhao, E.-G. Zhao and S.-G. Zhou, Phys. Scripta **89**, 054028 (2014).

[50] B.-N. Lu, J. Zhao, E.-G. Zhao and S.-G. Zhou, EPJ Web Conf. **38**, 05003 (2012).

[51] J. Zhao, B.-N. Lu, D. Vretenar, E.-G. Zhao and S.-G. Zhou, Phys. Rev. C **91**, 014321 (2015).

[52] J. Zhao, B.-N. Lu, T. Nikšić, D. Vretenar and S.-G. Zhou, Phys. Rev. C **93**, 044315 (2016).

[53] J. Zhao, B.-N. Lu, E.-G. Zhao and S.-G. Zhou, Phys. Rev. C **86**, 057304 (2012).

[54] B.-N. Lu, E.-G. Zhao and S.-G. Zhou, Phys. Rev. C **84**, 014328 (2011).

[55] B.-N. Lu, E. Hiyama, H. Sagawa and S.-G. Zhou, Phys. Rev. C **89**, 044307 (2014).

[56] L.-L. Li, B.-N. Lu, N. Wang, K. Wen, C.-J. Xia, Z.-H. Zhang, J. Zhao, E.-G. Zhao and S.-G. Zhou, Nucl. Phys. Rev. **31**, 253 (2014) (*in Chinese*).

[57] B.-N. Lu, J. Zhao, E.-G. Zhao and S.-G. Zhou, *Superheavy nuclei and fission barriers*, in *Relativistic density functional for nuclear structure, chap. 5*, ed. J. Meng, Int. Rev. Nucl. Phys. **10**, 171. World Scientific, 2016.

[58] Y. Tian and Z.-Y. Ma, Chin. Phys. Lett. **23**, 3226 (2006).

[59] Y. Tian, Z. Y. Ma and P. Ring, Phys. Lett. B **676**, 44 (2009).

[60] Y. Tian, Z.-Y. Ma and P. Ring, Phys. Rev. C **80**, 024313 (2009).

[61] T. Nikšić, D. Vretenar and P. Ring, Phys. Rev. C **78**, 034318 (2008).

[62] T. Nikšić, P. Ring, D. Vretenar, Y. Tian and Z.-Y. Ma, Phys. Rev. C **81**, 054318 (2010).

[63] J. Zhao, B.-N. Lu, T. Nikšić and D. Vretenar, Phys. Rev. C **92**, 064315 (2015).

[64] J. Zhao, B.-N. Lu, E.-G. Zhao and S.-G. Zhou, Phys. Rev. C **95**, 014320 (2017), arXiv:1606.08994 [nucl-th] (2016).

[65] B. D. Serot and J. D. Walecka, Adv. Nucl. Phys. **16**, 1 (1986).

[66] P. G. Reinhard, Rep. Prog. Phys. **52**, 439 (1989).

[67] P. Ring, Prog. Part. Nucl. Phys. **37**, 193 (1996).

[68] M. Bender, P.-H. Heenen and P.-G. Reinhard, Rev. Mod. Phys. **75**, 121 (2003).

[69] D. Vretenar, A. V. Afanasjev, G. A. Lalazissis and P. Ring, Phys. Rep. **409**, 101 (2005).

[70] J. Meng, H. Toki, S. G. Zhou, S. Q. Zhang, W. H. Long and L. S. Geng, Prog. Part. Nucl. Phys. **57**, 470 (2006).

[71] N. Paar, D. Vretenar and G. Colo, Rep. Prog. Phys. **70**, 691 (2007).

[72] T. Nikšić, D. Vretenar and P. Ring, Prog. Part. Nucl. Phys. **66**, 519 (2011).

[73] H. Liang, J. Meng and S.-G. Zhou, Phys. Rep. **570**, 1 (2015).

[74] J. Meng and S. G. Zhou, J. Phys. G **42**, 093101 (2015).

[75] J. Boguta and A. R. Bodmer, Nucl. Phys. A **292**, 413 (1977).

[76] R. Brockmann and H. Toki, Phys. Rev. Lett. **68**, 3408 (1992).

[77] Y. Sugahara and H. Toki, Nucl. Phys. A **579**, 557 (1994).

[78] B. A. Nikolaus, T. Hoch and D. G. Madland, Phys. Rev. C **46**, 1757 (1992).

[79] T. Burvenich, D. G. Madland, J. A. Maruhn and P.-G. Reinhard, Phys. Rev. C **65**, 044308 (2002).

[80] C. Fuchs, H. Lenske and H. H. Wolter, Phys. Rev. C **52**, 3043 (1995).

[81] T. Nikšić, D. Vretenar, P. Finelli and P. Ring, Phys. Rev. C **66**, 024306 (2002).

[82] J. Meng (ed.) *Relativistic density functional for nuclear structure*, Int. Rev. Nucl. Phys. **10**. World Scientific, 2016.

[83] H. Kucharek and P. Ring, Z. Phys. A **339**, 23 (1991).

[84] Y. K. Gambhir, P. Ring and A. Thimet, Ann. Phys. (NY) **198**, 132 (1990).

[85] P. W. Zhao, Z. P. Li, J. M. Yao and J. Meng, Phys. Rev. C **82**, 054319 (2010).